Korean J. Chem. Eng., 40(4), 873-881 (2023)
DOI: 10.1007/s11814-022-1230-0

pISSN: 0256-1115
eISSN: 1975-7220

Methylene blue adsorption by wheat straw-based adsorbents: Study of adsorption kinetics and isotherms

Somayeh Mohamadi Sodkouieh*,, Maryam Kalantari*,†, and Tayebeh Shamspur***

*Department of Chemistry, Shahid Bahonar University of Kerman, Kerman, Iran
**Young Research Society, Shahid Bahonar University of Kerman, Kerman, Iran
(*Received 12 May 2022 • Revised 7 July 2022 • Accepted 13 July 2022*)

Abstract−Dyes are one of the major toxic pollutants discharged in large quantities into the hydrosphere. Among various dye removal methods, adsorption has a distinct position. In this study, wheat straw was used as a low-cost and renewable material to prepare two economical adsorbents through the facile production method. An adsorbent was prepared by alkaline hydrolysis of wheat straw. Then, another adsorbent was synthesized by carboxymethylation of the first adsorbent. The prepared adsorbents were characterized by various techniques, including Fourier transform infrared spectroscopy (FT-IR), field-emission scanning electron microscopy (FESEM), and X-ray diffraction (XRD). A series of adsorption experiments were conducted in a batch adsorption system to study the effect of diverse parameters, such as solution pH, the initial dye concentration, and contact time, on the adsorption performance. Adsorption models and kinetic results indicated that the adsorption of methylene blue onto both adsorbents was more fitted to Langmuir isotherm and followed second-order kinetics. The maximum monolayer adsorption capacity of methylene blue on alkaline-modified wheat straw and carboxymethylated modified wheat straw reached 131.123 and 191.427 mg/g, respectively. Regarding their low cost and suitable adsorption potential, they can be cost-effective and promising adsorbents for wastewater treatment.

Keywords: Adsorption, Dye Removal, Water Treatment, Wheat Straw, Methylene Blue

INTRODUCTION

With the increasing population and technology growth, our world moves towards new horizons. In the contemporary period, the water demand has dramatically increased. Saving water resources to ensure future water security is needed now more than ever. Agricultural, industrial, and domestic sectors generate large amounts of effluents containing various pollutants. Dyes are one of the most important categories of contaminations [1]. Most dyes are organic molecules whose structural complexity makes them resistant to light, water, detergents, and chemicals, further challenging the decolorization of contaminated water [2]. The dyeing, textile, paper, leather tanning, cosmetics, and rubber industry are the primary consumers of synthetic dyes. Therefore, the effluents of these industries contain significant amounts of dye [3,4]. These toxic chemicals have shown carcinogenic, teratogenic, and mutagenic effects on aquatics, and humans. Moreover, dyes reduce sunlight penetration and disrupt biological metabolic processes, destroying aquatic ecosystems [5,6]. In this context, the development of safe, low-cost, and facile methods to treat dye-contaminated effluents is highly welcome. Several methods have been proposed to treat dye-bearing effluents that can be divided into three general categories: chemical, physical, and biological [7]. Each of these methods has its specific advantages and disadvantages.

Among various methods, adsorption has found a special position in dye removal. It is a physicochemical process of wastewater treatment involving the separation of adsorbates from an aqueous phase to a solid phase. Adsorption has several advantages over other wastewater treatment methods: simple operation, high efficiency, and relatively reasonable cost [8,9]. The adsorbent is one of the most essential factors in an adsorption system. A suitable adsorbent is low-cost while offering a high adsorption capacity. Activated carbon (AC), the most commonly used adsorbent, has a high adsorption capacity, but its production cost is very high. Therefore, numerous studies have recently addressed the development of a low-cost alternative adsorbent [10]. Some agricultural wastes can serve as low-cost and available adsorbents. However, many of these raw materials have limited application due to their tendency to release water-soluble organic components and the lack of suitable functional groups [11,12]. Some techniques have been proposed to overcome this problem. One of them is the carbonization of agricultural by-products [13]. Biochar (BC) is a solid substance which can be obtained by biomass carbonization. BC has more oxygen-containing functional groups (such as C-O and C=O) than AC [14,15]. Due to the wide availability of its initial materials, BC may be prepared from the direct burning of its precursors, making BC production less expensive than AC. In addition, BCs often show much higher adsorption capacity for dyes and some other water pollutants than the initial biomass due to their higher porosity and increased surface area [16]. Another technique is the chemical modification and introduction of suitable functional groups on raw agricultural by-products [11,12]. In recent years, different chemical treat-

†To whom correspondence should be addressed.
E-mail: kalantari@uk.ac.ir

ments were applied to the raw plant materials such as wheat straw [11], barley straw [17], sawdust, pine tree leaves [18], mango seeds [19], sesame straw [20], and rice straw [21] to improve their adsorption capacity.

In the present work, an attempt was made to chemically modify and introduce the ionic groups onto the surface of wheat straw (WS) to enhance its adsorption capacity toward ionic dyes. Wheat is one of the most abundant and widely distributed grains in the world. Wheat straw is one of the inexpensive and abundant by-products of wheat. Hundreds of millions of tons of WS are produced annually, most of which are burned or left on agricultural lands to decompose. However, raw WS has a low dye adsorption capacity. WS is primarily composed of cellulose, hemicellulose, and lignin. Its few suitable functional groups are not accessible due to its structural complexity [11,22]. This research is aimed to provide products with higher adsorption capacity through simple chemical modifications and partial removal of lignin, porosity enhancement, making suitable functional groups accessible, and introduction of new functional groups. In general, this article pursues several goals: Preparation of a cost-effective adsorbent with sufficient adsorption capacity from wheat straw waste, studying the performance of the synthesized adsorbents in the removal of methylene blue in a batch adsorption system, investigation of various parameters affecting the adsorption performance, adopting several adsorption models to fit the experimental data.

MATERIALS AND METHODS

1. Materials

Wheat straw was collected from a wheat field in Kerman province. After washing, it was dried in an oven at 60 °C for 24 hours, then crushed and ground, and sieved into a 40-mesh sieve. Methylene blue (MB), NaOH, HCl, and monochloroacetic acid (MCA) were purchased from commercial sources and used without further purification.

2. Preparation of Adsorbents

2-1. Preparation of Modified Wheat Straw (MWS)

First, 12 g of raw wheat straw was poured into a two-liter beaker containing 800 ml NaOH 12% W/W and stirred magnetically for 200 min at 60 °C [23]. During this time, the soluble materials in the alkaline medium were separated from the straw and the color of the solution turned dark brown. Finally, the water was separated from the straws by filtration and fresh distilled water was poured instead. Then, the pH was adjusted to 7 by adding 0.1 M HCl. Afterward, the MWS was washed once with water and twice with a mixture of water and ethanol (1 : 1). The produced MWS was dried in the oven at 45 °C for 24 h.

2-2. Preparation of Carboxymethylated Modified Wheat Straw (CMMWS)

To prepare CMMWS, first, 4 g of MWS was stirred in 230 ml of 3% w/w NaOH solution in a beaker at 60 °C for 1 h. Then, 10 g of MCA was added, and the reaction was continued for another 3.5 h at the same temperature [24]. Water was filtered, fresh water was added, and the pH was neutralized by adding 0.1 M HCl. The washing and purification steps were performed similarly to the case of MWS. The preparation process of the adsorbents is illustrated in Scheme 1.

3. Instrumentation

The FTIR characterization of the raw WS, MWS, and CMMWS was recorded at 4,000-400 cm^{-1} on a JASCO FT-IR 300E spectrophotometer. The surface morphology of the samples was examined by FESEM-EDX (Zeiss, Sigma, Germany). Given that the samples lacked conductivity, they were coated with gold before use in this test. The X-ray diffraction (XRD) pattern of the samples was obtained using a Bruker AXS model D8 advance diffractometer with Cu-Kα radiation in the scan range of 2θ=7-80° (λ=1.5048 A°) at room temperature (25 °C). The dye concentration in an aqueous solution was measured using a UV-VIS double-beam spectrometer (SQ2810E, UNICO, Germany) by monitoring the absorbance changes at a wavelength of maximum absorbance (663 nm) [25].

4. Batch Adsorption Experiments

A stock solution (500 mg/L) of MB was prepared by dissolving a precisely measured quantity of dye in distilled water. Other concentrations were prepared by diluting this solution with distilled water. Fig. 1 illustrates the chemical structure of MB [26]. All adsorption experiments were conducted with 0.02 g of adsorbent in

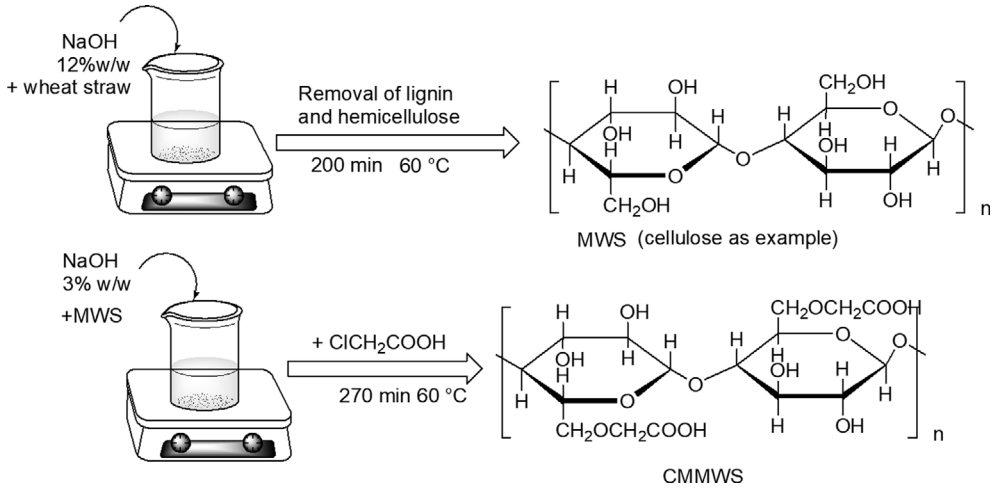

Scheme 1. Preparation of adsorbents.

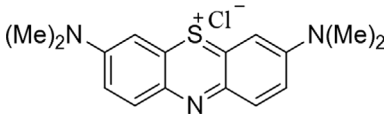

Fig. 1. Chemical structure of methylene blue.

45 ml of adsorbate solution (5-150 mg/L) in a sealed 50 ml glass bottle at room temperature and a known pH under stirring at 300 rpm. Noteworthy, all experiments were performed in duplicate. At the final stage, the solution was separated from the adsorbent by centrifugation and diluted if necessary (to obtain absorbance within the linear calibration range). The absorption was measured by the UV-visible spectrophotometer.

4-1. pH Effect on MB Adsorption

The effect of MB solution pH on dye removal was explored by preparing solutions with different pHs (3, 5, 7, and 9). The solution pH was adjusted by 0.1 M HCl or NaOH. In this experiment, the contact time was 160 min, and the initial dye concentration was set to 10 mg/L. The removal efficiency (%R_E) of the dye can be calculated by Eq. (1):

$$\%R_E = \frac{(C_0 - C_t)100}{C_0} \quad (1)$$

where C_0 and C_t (mg/ L) are the dye concentrations at the initial time and at the time of t, respectively.

4-2. Adsorption Isotherms and Kinetic Studies

Adsorption isotherm experiments were performed for MB solutions with different concentrations (5, 10, 20, 30, 50, 75, 100, and 150 mg/L) at pH=7 and a contact time of 140 min. Kinetic experiments were conducted using a dye solution with an initial concentration of 100 mg/L and pH=7 at different times (20, 40, 80, 120, and 160 min) using separate bottles. The removal efficiency (%R_E) of the dye was determined by Eq. (1).

The amount of dye adsorbed by the unit weight of adsorbent (q_t or q_e, mg/ g) can be calculated via Eq. (2):

$$q = \frac{(C_0 - C)V}{m} \quad (2)$$

where C_0 is the initial MB concentration (mg/L), C denotes dye concentration at any time of t or equilibrium (mg/ L), V is the volume of solution (L), and m is the mass of adsorbent (g).

5. Desorption of MB from Adsorbents

In the first step (adsorption step), 45 ml of dye solution (100 mg/L) and 0.02 g of adsorbent (MWS or CMMWS) were poured into six glass bottles separately. They were agitated for 5 h and then the dye-loaded adsorbent was filtered off and dipped in different solutions (HCl 0.01 M, NaCl 0.01 M, and distilled water) on the stirrer for 5 h. Finally, the solution was separated from the adsorbent and the desorbed dye concentration was determined.

RESULTS AND DISCUSSION

1. Characterization of the Adsorbent

FTIR spectra of WS, MWS, and CMMWS were investigated to compare the different modifications. As depicted in Fig. 2(a), the

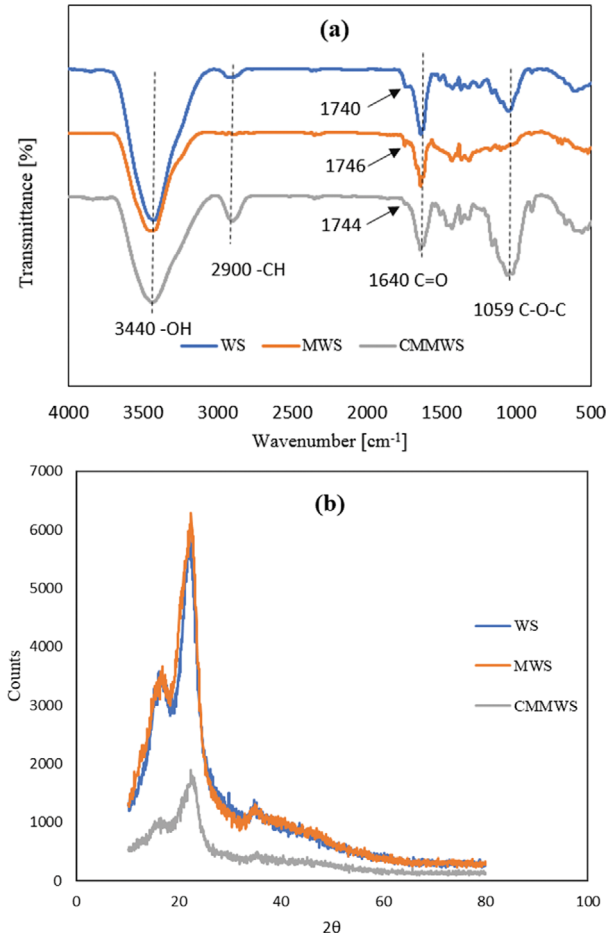

Fig. 2. (a) FTIR spectra, and (b) XRD spectra of WS, MWS, and CMMWS.

strong peak at around 3,200-3,600 cm^{-1} corresponds to the stretching vibration of O-H [27], while the adsorption bands at 2,918 and 1,372 cm^{-1} can be assigned to C-H stretching and bending vibrations of the methylene groups [28]. The absorption band at around 1,740 cm^{-1} in the WS can be attributed to either the acetyl and uronic ester groups of the hemicelluloses or the ester linkage of the carboxylic group of the poumeric and ferulic acids of lignin and hemicelluloses [29]. The peak at 1,642 cm^{-1} is associated with the carbonyl group of the carboxylic acid with an intermolecular hydrogen bond [28]. The asymmetric stretching vibration of C-O-C appeared at 1,058 cm^{-1}. In the case of MWS, almost all absorption bands are shorter than in the spectrum of WS. This decrease can be attributed to the dissolving of compounds such as solvable organic materials of the straw structure, hemicellulose, and lignin [28,30]. In the CMMWS spectrum, the stretching vibrations of the OH group appear with a broader peak (3,000-3,600 cm^{-1}), indicating an increase in the acidic OH groups. Furthermore, the bands at ~900, 1,060, 1,300, and 1,430 cm^{-1} can be attributed to the carboxymethyl groups, showing significant increases after carboxymethylation [31,32]. These results confirmed the successful carboxymethylation with mono chloroacetic acid.

XRD patterns of WS, MWS, and CMMWS are shown in Fig. 2(b). Three typical diffractions of cellulosic material at diffraction

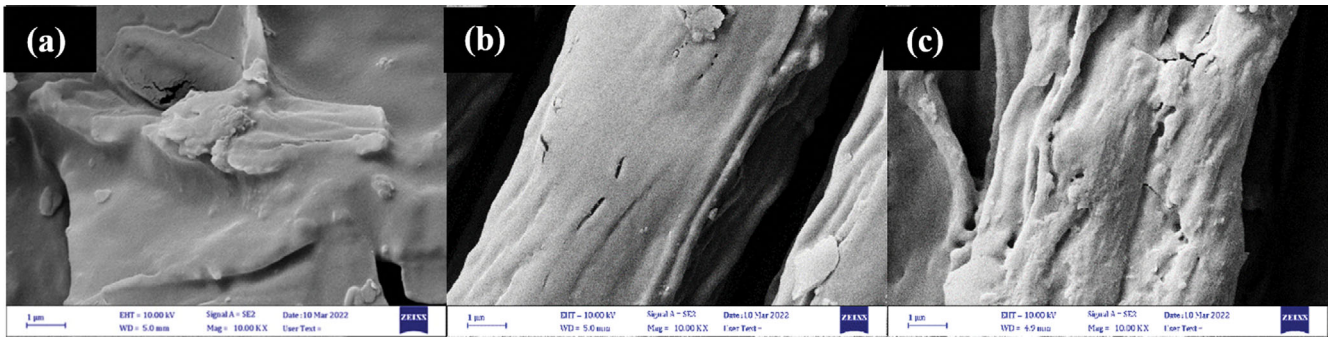

Fig. 3. SEM of (a) pure WS, (b) MWS, and (c) CMMWS.

angles of 15.1°, and 21.9°, and 35.2° appeared in the XRD pattern of WS confirming that the cellulose form is cell-I. The crystalline portion led to the highest intensity peak, whereas the noise lines are due to the amorphous fraction [31]. Comparing the XRD patterns of WS and MWS, there is a minor change. Thus, it can be concluded that the main backbone structure of WS remained stable during alkaline hydrolysis. Whereas the carboxymethylation reaction on the cellulose structure decreased the crystallinity. These results are parallel to earlier results [33,34].

The FESEM images of the adsorbents in Fig. 3(a)-(c) exhibit different morphological properties of the adsorbents. As can be seen in Fig. 3(a), (b), the surface of MWS has more porosity than pure WS, which might be due to the removal of lignin and hemicellulose through alkaline hydrolysis. Fig. 3(c) shows a more significant increase in pores and roughness, suggesting a rise in the specific surface area, hence improving the adsorption capacity of CMMWS compared to the other adsorbents [11,29].

2. Adsorption Property of MWS and CMMWS for MB

2-1. pH Effect

One of the most critical factors affecting the adsorption process is the pH of the solution as the charge of the adsorbate and adsorbent usually depends on the solution pH [35]. In this experiment, the effect of pH was studied at various pH levels ranging from 3 to 9 (Fig. 4). The general form of the diagram shows the same dye removal ability of two adsorbents in all pHs, except at pH=3. At this pH, the $\%R_E$ was estimated to be 66.5% for CMMWS and 38% for the MWS. The studied adsorbents are cellulose-based and encompass hydroxy and carboxylic acid groups. These groups will be protonated under concentrated acidic conditions. Therefore, positive sites are created on the adsorbent structure. Electrostatic repulsion occurs between these positive sites with MB as a cationic dye [11]. Thus, the dye molecules cannot be well adsorbed on the adsorbent at this pH. MWS has more hydroxy groups than CMMWS because some of these groups have been converted into OCH_2COOH during the carboxylation reaction and preparation of CMMWS. Thus, the lower $\%R_E$ of MWS at this pH may be due to the greater potential of OH groups for protonation (owing to the localized electrons of oxygen) rather than COOH [36], resulting in more positive sites and greater electrostatic repulsion between the adsorbent and MB. In the following, it can be seen that for both adsorbents, the removal efficiency increased with pH elevation from 3 to 7 at a large slope. As hydroxy and carboxylic acid groups on adsorbents structure were deprotonated at pH=7 or higher, the cationic molecules of MB can be well adsorbed on an anionic adsorbent. So, this process is normal and logical. Also, $\%R_E$ was slightly better at pH=7 compared to pH=9. This can be explained by the fact that at too high pH, the number of hydroxide ions in the solution is high; these ions surround the dye structure and reduce its electrostatic attraction to the adsorbent [37]. Since the highest dye removal occurred at pH 7.0, further studies were performed at this pH.

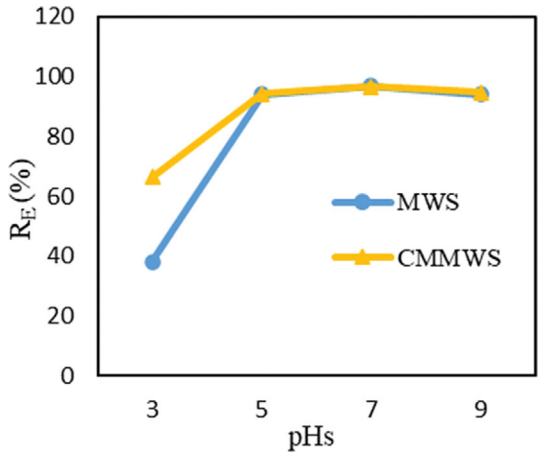

Fig. 4. pH effect on MB adsorption onto MWS, CMMWS (Conditions: initial dye concentration=10 mg/L, contact time=160 min).

2-2. Initial Concentration Effect and Adsorption Isotherm

The adsorption capacity was assessed by varying the MB initial concentration (5-150 mg/L). For both adsorbents, the adsorption was increased by enhancing the dye concentration (Fig. 5(a)). At low concentrations (5, 10, 20 mg/L), both adsorbents removed more than 90% of the dye, showing almost the same adsorption capacity. An increase in the dye concentration enhanced the difference in adsorption capacity of the two adsorbents. Adsorption isotherms are an essential part of describing the adsorbent-adsorbate interactions [38]. For this purpose, Langmuir, Freundlich, and Temkin isotherm models were considered in the presented study. The linear form of these isotherms equations is listed in Table 1. The fitted plots of Langmuir, Freundlich and Temkin isotherm models are also presented in Fig. 5(b)-(d), while their corresponding calculated parame-

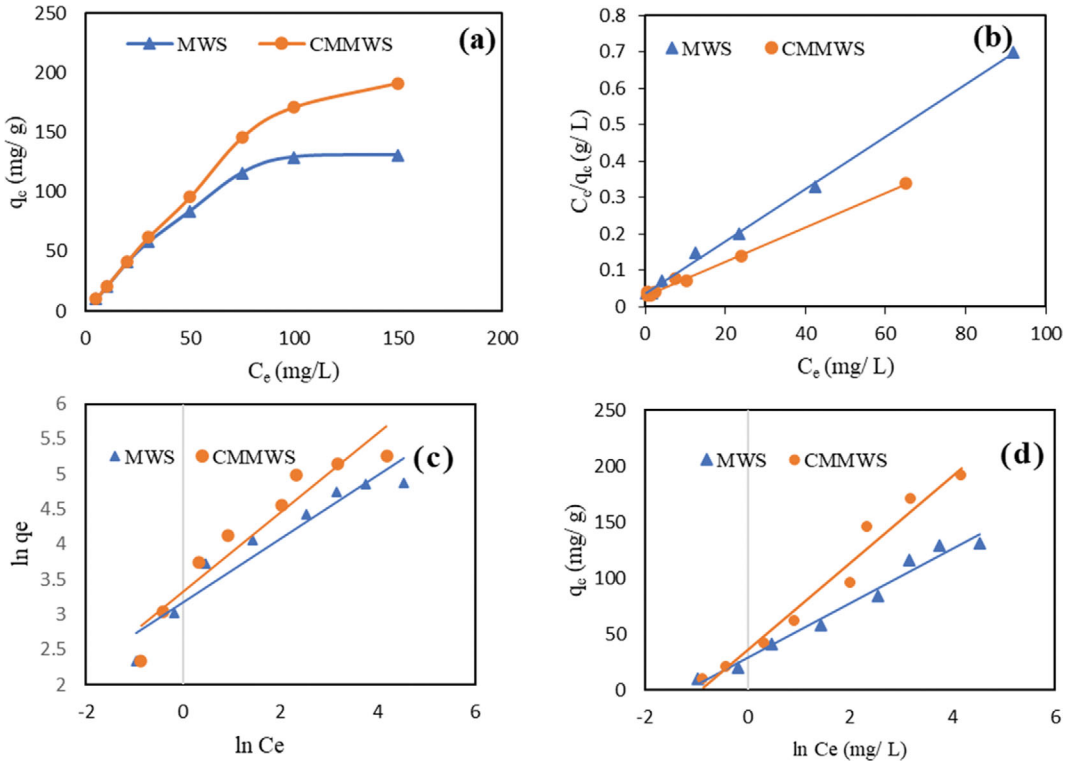

Fig. 5. (a) Effect of initial concentration, linear fitting data for (b) Langmuir, (c) Freundlich, and (d) Temkin isotherm for MB adsorption onto MWS and CMMWS adsorbents (Conditions: initial dye concentration=5-150 mg/L, contact time=160 min pH=7).

Table 1. Isothermal and kinetic models used in this study

	Model	Linear form
Isotherm models	Langmuir	$\frac{C_e}{q_e}=\frac{1}{K_l q_m}+\frac{C_e}{q_m}$, $R_L\frac{1}{1+K_L C_0}$
	Freundlich	$\ln q_e=K_f+\frac{1}{n}\ln C_e$
	Temkin	$q_e=B\ln A+B\ln C_e$
Kinetic models	Pseudo-first order	$\ln(q_e-q_t)=\ln q_e-k_1 t$
	Pseudo-second order	$\frac{t}{q_t}=\frac{1}{K_2 q_e^2}+\frac{t}{q_e}$
	Intraparticle diffusion	$q_t=K_P t^{0.5}+C$

Where C_e (mg/L), q_e (mg/g), K_l (L/ mg), and q_m (mg/g) denote the dye concentration in equilibrium, the adsorption capacity in equilibrium, the Langmuir constant, and the maximum capacity of the adsorption, respectively. R_L is the separation factor, K_f (L/mg), and n are Freundlich constants. A and B are also Temkin constants; t (min) shows the time, while K_1, K_2, and K_p (mg/g $min^{0.5}$) are the rate constants of pseudo-first, second-order, and intraparticle diffusion, respectively, q_t (mg/g) is the adsorption capacity at the time of t.

ters are listed in Table 2. Among the employed models, the Langmuir model was the most appropriate model to describe the adsorption of MB on the adsorbents due to its highest R^2. Langmuir model denotes the monolayer coverage of the dye onto adsorbents (R^2= 0.997 for MWS, and R^2=0.995 for CMMWS) [39]. The maximum adsorption capacity of MWS and CMMWS was 138.888, and 212.766 mg/g, respectively, which are close to the experimental value of q_m (131.123, 191.427 mg/g). The higher adsorption capacity of CMMWS can be attributed to the excellent adsorption ability of the carboxylate groups of CMMWS toward MB cationic molecules through higher electrostatic interaction [40]. However, the larger porosity of CMMWS that is conducive to the easier diffusion of dye molecules to the interior can be considered as another reason for the increase in the adsorption capacity of this adsorbent [41]. The values of the separation factor (R_L) were calculated at different initial concentration ($0<R_L<1$), revealing that the MB adsorption onto the adsorbents is favorable [42]. On the other hand, at higher concentration, the value of R_L approached zero, indicating the irreversibility of the adsorption process. Furthermore, the Freundlich constant of both adsorbents varied in $0<1/n<1$, indicating a proper

Table 2. Isotherm parameters for the adsorption of MB by MWS and CMMWS

Isotherm models	Parameters	MWS	CMMWS
Langmuir	$q_{m\ exp}$ (mg/g)	131.123	191.427
	$q_{m,\ cal}$ (mg/g)	138.888	212.766
	K_L (L/mg)	0.197	0.152
	R^2	0.997	0.995
	$R_L{}^a$	0.845	0.866
	$R_L{}^b$	0.154	0.177
Freundlich	K_f (L/mg)	24.063	27.640
	1/n	0.452	0.568
	R^2	0.919	0.910
Temkin	B (J/mol)	24.321	38.881
	A (L/mg)	3.340	2.506
	R^2	0.977	0.967

[a]Initial dye concentration of 5.0 mg/L
[b]Final dye concentration of 150 mg/L

adsorption process [43]. Furthermore, the data showed a relatively good agreement with the Temkin model, suggesting adsorbent-MB electrostatic interaction as one of the contributing mechanisms [44].

2-3. Effects of the Contact Time and Kinetics

The effect of contact time on MB adsorption onto MWS and CMMWS was investigated (Fig. 6(a)). Since the adsorption capacity of MWS for 100 and 150 (mg/L) concentrations were too close to each other, to obtain a better comparison, the experiments were continued with an initial concentration of 100 (mg/L). In the case of CMMWS, a three-step adsorption process occurred: an initial rapid increase (0-40 min), the subsequent slow improvement (40-80 min), and relative balance in the adsorption capacity rate (80-160 min). Whereas two adsorption steps can be observed in the case of MWS: A moderate increase in adsorption capacity rate (0-80 min) followed by slow growth (80-160 min). Indeed, no fast start stage occurred like what happened for CMMWS. At the end of 160 minutes, the R_E of MWS and CMMWS was estimated to be 57.49% and 76.06%, respectively. Note that the adsorption capacity of adsorbents after 160 minutes showed a negligible increase, which was ignored. The study of adsorption kinetics is a common analytical method for comprehending the adsorption mechanism. In the present study, pseudo-first-order and pseudo-second-order, and intraparticle diffusion models were used to fit the experimental data. The linear forms of these kinetic equations are presented in Table 1 [42]. Based on the fitted plots (Fig. 6(b)-(d)) and the corresponding kinetic parameters (Table 3), the MB adsorption over MWS and CMMWS was more adapted to the pseudo-second-order kinetic model as the q_e values calculated from this model were closer to the experimental q_e results. Meanwhile, R^2 values obtained from this kinetic model were closer to unity (R^2>0.992 for both adsorbents). Accordingly, it can be concluded that chemisorption is the main rate-limiting step for MB adsorption onto the adsor-

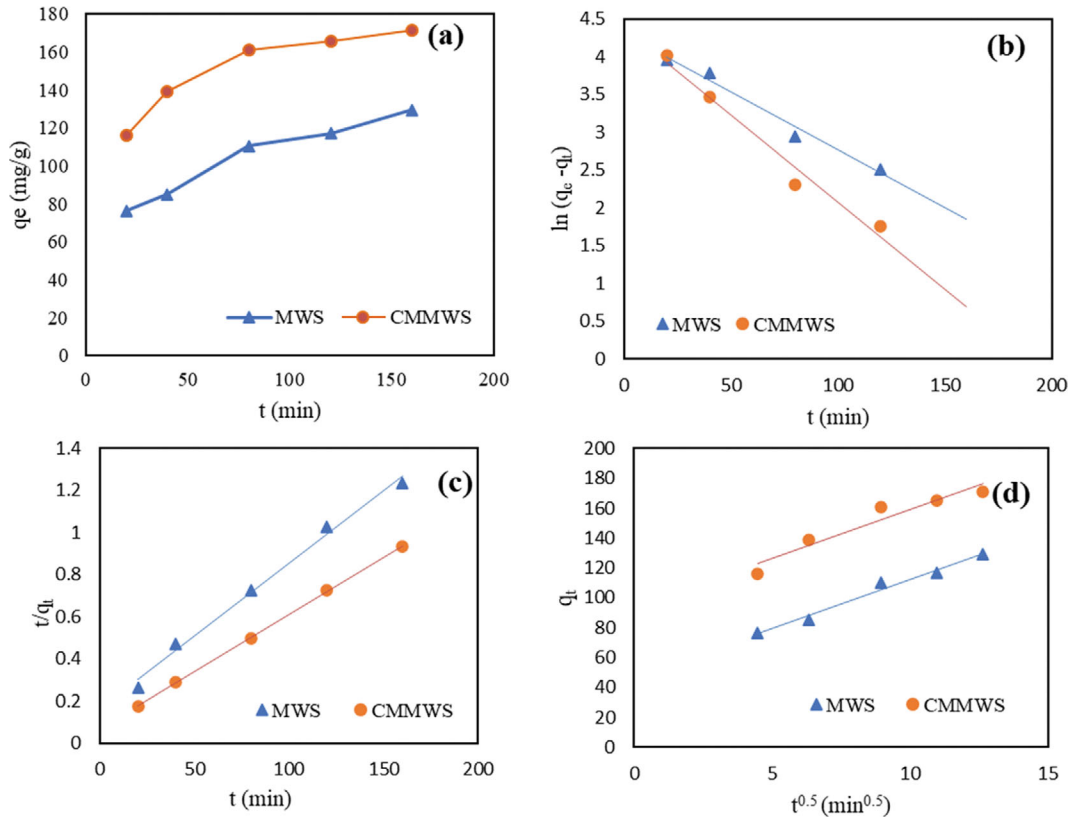

Fig. 6. (a) Effect of contact time, and linear fitting kinetics model (b) Pseudo-first-order, (c) Pseudo-second-order, and (d) intra-particle diffusion for MB adsorption towards MWS, and CMMWS adsorbent (Conditions: initial dye concentration=100 mg/L, contact time=20-160 min pH=7).

Table 3. Kinetic parameters for adsorption of MB by MWS and CMMWS

Kinetic models	Parameters	MWS	CMMWS
Pseudo-first-order	$q_{m\ exp}$ (mg/g)	129.375	177.141
	$q_{e,1}$ (mg/g)	73.398	80.366
	k_1 (min^{-1})	0.015	0.023
	R^2	0.980	0.975
Pseudo-second-order	$q_{e,2}$ (mg/g)	144.927	185.185
	K_2 (min^{-1})	0.0419	0.0819
	R^2	0.992	0.998
Intraparticle diffusion	K_p (mg/g·$min^{0.5}$)	6.611	6.578
	C (mg/g)	46.312	93.457
	R^2	0.981	0.919

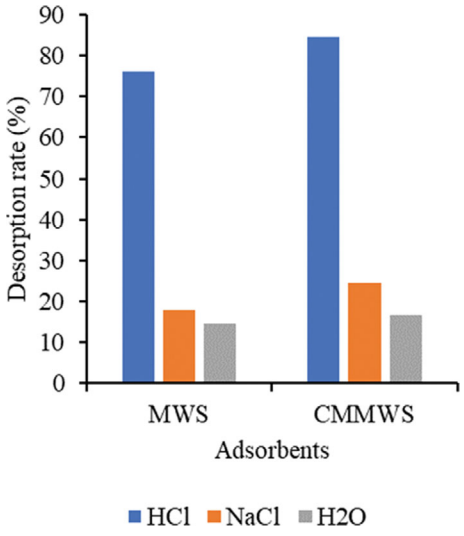

Fig. 7. Desorption rate of MB from the dye-loaded adsorbents in different solutions (Concentration: 0.01 mol/L).

bents [40]. Furthermore, the k_2 values of MB adsorption onto MWS and CMMWS were 0.0419 and 0.0819 (min^{-1}), respectively. This means the adsorption rate of CMMWS was nearly twice faster as that of MWS [39]. None of the C values calculated by the intraparticle diffusion kinetic equation were zero, suggesting that the surface adsorption and film diffusion might affect and control the reaction rate [44,45]. Note that raw wheat straw was tested under optimal conditions (i.e., pH=7, initial concentration of 100 mg/L, contact time=160 min) and its adsorption capacity and R_E were 58.44 mg/L and 25.97%, respectively.

3. Desorption of MB

Fig. 7 shows the effect of the different mediums (HCl, NaCl and H_2O) on the desorption rate of MB dye. The best desorption occurred in the HCl solution. Moreover, the desorption was more significant in the NaCl solution than in distilled water, reflecting the decisive role of ion exchange and inter-ion electrostatic attraction in the adsorption mechanism of MB [20]. A 60% enhancement in the desorption in the acid solution compared to the NaCl solution can be attributed to the protonation of the hydroxy and carboxylic acid groups on the structure of the adsorbents. An

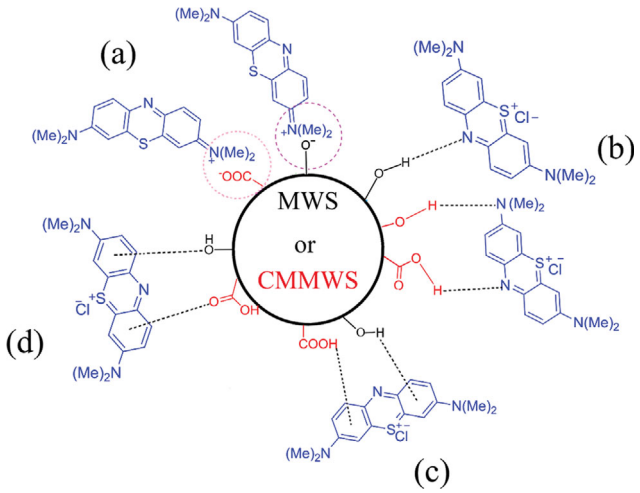

Scheme 2. Illustration of the possible interaction mechanism between adsorbents and MB dye: (a) Electrostatic interactions, (b) dipole-dipole H-bonding interactions, (c) Yoshida H-bonding, and (d) n-π stacking interactions.

increment in the positive charge on the adsorbent structure can increase the MB dye desorption efficiency due to the electrostatic repulsion between positively charged sites on the adsorbent structure and cationic dyes [12,46].

4. Adsorption Mechanism

The adsorption mechanism of MB on the surface of the adsorbents is governed by different types of interactions, as shown in Scheme 2. Electrostatic attractions can be considered as one of the most critical attraction forces between adsorbents and MB [47,48]. Two functional groups (COOH and OH) onto MWS and CMMWS, in solution, can lose their protons and form a potential negative surface for the adsorption of cationic dyes (here, MB) [5]. The adsorption mechanism also includes two types of hydrogen bonding: H-bonding between OH and COOH groups on the adsorbents surface with 1) oxygen and nitrogen of MB structure (dipole-dipole H-bonding) and 2) the aromatic ring of dye (Yoshida H-bonding) [49]. The n-π interaction is the other one that occurs through the delocalization of the nonbonding electron pair of the oxygen atoms into the π orbital of the aromatic ring [50].

5. Comparative Study

The MB adsorption capacities of CMMWS and MWS were compared with various adsorbents as listed in Table 4. The adsorption capacity of the dye onto the prepared adsorbents (especially CMMWS) is higher than that of many other previously reported adsorbents, suggesting their feasibility and applicability as a convenient, low-cost, and effective adsorbent for wastewater treatment.

CONCLUSION

MWS adsorbent was prepared by alkaline hydrolysis of WS, and CMMWS was synthesized from carboxymethylation of MWS through reacting with monochloroacetic acid. The maximum monolayer adsorption capacity of MB on MWS and CMMWS reached 131.123 and 191.427 mg/g, respectively, indicating a 72% (for CMMWS) and 58% (for MWS) improvement over the primary

Table 4. Comparison of adsorption capacity of previously reported adsorbents for MB adsorption

Adsorbent	q_m (mg/g)	Reference
Cellulose-based biocomposite film	146.81	[48]
Xanthate-modified baker's yeast	64.45	[51]
Functionalized microcrystalline cellulose	115.20	[52]
FeCl3-pretreated rice straw	52.90	[28]
Carica papaya wood	32.25	[53]
Scenedesmus dimorphus	6.00	[54]
Activated spent tea	104.20	[55]
Jute stick derived activated carbon	384.60	[56]
Tartaric acid modified wheat straw	129.87	[57]
Wheat straw biochar	62.50	[58]
Cedrela odorata L seed biochar	158.8	[59]
NaOH modified wheat straw (MWS)	131.123	Present work
Carboxymethylated modified wheat straw (CMMWS)	191.427	Present work

straw. The superior adsorption capacity of CMMWS could be attributed to the ability of the carboxylate groups to adsorb dye cationic molecules through high electrostatic interaction, which also justifies the faster dye removal rate of CMMWS compared to MWS. The Langmuir model properly matched isotherm data, and the pseudo-second-order kinetic model best fitted the kinetic findings. Thus, ion exchange and chemisorption are responsible for the adsorption of the dye. Regarding the availability and low cost of the initial material and the facile production route, the CMMWS can be a promising and effective adsorbent for wastewater treatment.

ACKNOWLEDGEMENTS

The authors gratefully acknowledge the financial support of the Shahid Bahonar University of Kerman.

REFERENCES

1. V. K. Gupta, *J. Environ. Manage.*, **90**, 2313 (2009).
2. T. Robinson, B. Chandran and P. Nigam, *Bioresour. Technol.*, **85**, 119 (2002).
3. V. Katheresan, J. Kansedo and S. Y. Lau, *J. Environ. Chem. Eng.*, **6**, 4676 (2018).
4. A. Arabpour, S. Dan and H. Hashemipour, *Arab. J. Chem.*, **14**, 103003 (2021).
5. Y. Su, B. Zhao, W. Xiao and R. Han, *Environ. Sci. Pollut. Res.*, **20**, 5558 (2013).
6. S. P. Raghuvanshi, R. Singh, C. P. Kaushik and A. Raghav, *Appl. Ecol. Environ. Res.*, **2**, 35 (2004).
7. G. Crini, *Bioresour. Technol.*, **97**, 1061 (2006).
8. S. Qiao, Q. Hu, F. Haghseresht, X. Hu and G. Q. M. Lu, *Sep. Purif. Technol.*, **67**, 218 (2009).
9. S. Banivaheb, S. Dan, H. Hashemipour and M. Kalantari, *J. Saudi Chem. Soc.*, **25**, 101283 (2021).
10. S. Afroze and T. K. Sen, *Water, Air, Soil Pollut.*, **229**, 1 (2018).
11. H. You, J. Chen, C. Yang and L. Xu, *Colloids Surf. A Physicochem. Eng. Asp.*, **509**, 91 (2016).
12. M. J. Ahmed, B. H. Hameed and E. H. Hummadi, *J. Mol. Liq.*, **330**, 115616 (2021).
13. Y. Liu, X. Zhao, J. Li, D. Ma and R. Han, *Desalin. Water Treat.*, **46**, 115 (2012).
14. S. S. Lam, P. N. Y. Yek, Y. S. Ok, C. C. Chong, R. K. Liew, D. C. W. Tsang, Y.-K. Park, Z. Liu, C. S. Wong and W. Peng, *J. Hazard. Mater.*, **390**, 121649 (2020).
15. J.-Y. Kim, S. Oh and Y.-K. Park, *J. Hazard. Mater.*, **384**, 121356 (2020).
16. Y. Qiu, Z. Zheng, Z. Zhou and G. D. Sheng, *Bioresour. Technol.*, **100**, 5348 (2009).
17. S. Ibrahim, I. Fatimah, H.-M. Ang and S. Wang, *Water Sci. Technol.*, **62**, 1177 (2010).
18. M. T. Yagub, T. K. Sen and H. M. Ang, *Water, Air, Soil Pollut.*, **223**, 5267 (2012).
19. W. S. Alencar, E. Acayanka, E. C. Lima, B. Royer, F. E. de Souza, J. Lameira and C. N. Alves, *Chem. Eng. J.*, **209**, 577 (2012).
20. Y. Feng, Y. Liu, L. Xue, H. Sun, Z. Guo, Y. Zhang and L. Yang, *Bioresour. Technol.*, **238**, 675 (2017).
21. S. Sangon, A. J. Hunt, Y. Ngernyen, S. Youngme and N. Supanchaiyamat, *J. Clean. Prod.*, **318**, 128583 (2021).
22. T. S. Khan and U. Mubeen, *Curr. Res. J. Biol. Sci.*, **4**, 673 (2012).
23. C. Gao, J. Yang and L. Han, *Bioresour. Technol.*, **326**, 124786 (2021).
24. V. P. Chakka and T. Zhou, *Int. J. Biol. Macromol.*, **165**, 2425 (2020).
25. G. Liu, Z. Hu, R. Guan, Y. Zhao, H. Zhang and B. Zhang, *Korean J. Chem. Eng.*, **33**, 3141 (2016).
26. W. Zou, H. Bai, S. Gao and K. Li, *Korean J. Chem. Eng.*, **30**, 111 (2013).
27. Dan, S. Banivaheb, H. Hashemipour and M. Kalantari, *Polym. Bull.*, **78**, 1887 (2021).
28. I. Kim, M. S. U. Rehman and J.-I. Han, *J. Clean. Prod.*, **66**, 555 (2014).
29. Q. Lin, K. Wang, M. Gao, Y. Bai, L. Chen and H. Ma, *J. Taiwan Inst. Chem. Eng.*, **76**, 65 (2017).
30. B. Yu, G. Fan, S. Zhao, Y. Lu, Q. He, Q. Cheng, J. Yan, B. Chai and G. Song, *Appl. Biol. Chem.*, **64**, 1 (2021).
31. C. Aguir and M. F. M'Henni, *J. Appl. Polym. Sci.*, **99**, 1808 (2006).
32. H. Bidgoli, A. Zamani and M. J. Taherzadeh, *Carbohydr. Res.*, **345**, 2683 (2010).

33. A. Abdulhameed, *Microwave synthesis of Carboxymethylcellulose (CMC) from rice husk*, in: 13TH Int. Conf. (2020).
34. W. Klunklin, K. Jantanasakulwong, Y. Phimolsiripol, N. Leksawasdi, P. Seesuriyachan, T. Chaiyaso, C. Insomphun, S. Phongthai, P. Jantrawut and S. R. Sommano, *Polymers (Basel)*, **13**, 81 (2020).
35. Y. Wu, L. Zhang, C. Gao, J. Ma, X. Ma and R. Han, *J. Chem. Eng. Data*, **54**, 3229 (2009).
36. P. Vollhardt and N. Schore, *Organic chemistry: Structure and function*, Macmillan Learning publications, New York (2018).
37. M. Goyal, S. Singh and R. C. Bansal, *Carbon Lett.*, **5**, 170 (2004).
38. M. T. Yagub, T. K. Sen, S. Afroze and H. M. Ang, *Adv. Colloid Interface Sci.*, **209**, 172 (2014).
39. Z. Jia, Z. Li, T. Ni and S. Li, *J. Mol. Liq.*, **229**, 285 (2017).
40. K.-J. Hwang, W.-G. Shim, Y. Kim, G. Kim, C. Choi, S. O. Kang and D. W. Cho, *Phys. Chem. Chem. Phys.*, **17**, 21974 (2015).
41. K. Li, J. Yan, Y. Zhou, B. Li and X. Li, *J. Mol. Liq.*, **335**, 116291 (2021).
42. A. S. Eltaweil, H. A. Mohamed, E. M. Abd El-Monaem and G. M. El-Subruiti, *Adv. Powder Technol.*, **31**, 1253 (2020).
43. M. Verma, I. Tyagi, V. Kumar, S. Goel, D. Vaya and H. Kim, *J. Environ. Chem. Eng.*, **9**, 106045 (2021).
44. X. Yang, W. Zhu, Y. Song, H. Zhuang and H. Tang, *J. Mol. Liq.*, **340**, 116617 (2021).
45. S. Dan, M. Kalantari, A. Kamyabi and M. Soltani, *Polym. Bull.*, In press (2021).
46. E. Daneshvar, A. Vazirzadeh, A. Niazi, M. Kousha, M. Naushad and A. Bhatnagar, *J. Clean. Prod.*, **152**, 443 (2017).
47. S. Kocaman, *Int. J. Phytoremediation*, **22**, 551 (2020).
48. N. Somsesta, C. Piyamawadee, V. Sricharoenchaikul and D. Aht-Ong, *Korean J. Chem. Eng.*, **37**, 1999 (2020).
49. H. N. Tran, S.-J. You and H.-P. Chao, *Korean J. Chem. Eng.*, **34**, 1708 (2017).
50. A. H. Jawad, N. S. A. Mubarak and A. S. Abdulhameed, *J. Polym. Environ.*, **28**, 624 (2020).
51. M. Song, Z. Duan, R. Qin, X. Xu, S. Liu, S. Song, M. Zhang, Y. Li and J. Shi, *Korean J. Chem. Eng.*, **36**, 869 (2019).
52. H. Bai, J. Chen, X. Zhou and C. Hu, *Korean J. Chem. Eng.*, **37**, 1926 (2020).
53. S. Rangabhashiyam, S. Lata and P. Balasubramanian, *Surf. Interfaces*, **10**, 197 (2018).
54. T. S. Chandra, S. N. Mudliar, S. Vidyashankar, S. Mukherji, R. Sarada, K. Krishnamurthi and V. S. Chauhan, *Bioresour. Technol.*, **184**, 395 (2015).
55. A. A. Babaei, A. Khataee, E. Ahmadpour, M. Sheydaei, B. Kakavandi and Z. Alaee, *Korean J. Chem. Eng.*, **33**, 1352 (2016).
56. R. K. Ghosh, D. P. Ray, A. Tewari and I. Das, *Int. J. Environ. Sci. Technol.*, **18**, 2747 (2021).
57. R. Gong, Y. Liu, Y. Jiang and C. Li, *African J. Biotechnol.*, **8**, 7138 (2009).
58. G. Li, W. Zhu, C. Zhang, S. Zhang, L. Liu, L. Zhu and W. Zhao, *Bioresour. Technol.*, **206**, 16 (2016).
59. A. Subratti, J. L. Vidal, L. J. Lalgee, F. M. Kerton and N. K. Jalsa, *Sustain. Chem. Pharm.*, **21**, 100421 (2021).